Performance Prediction of Direct Torque-Controlled PMSM Drives Considering Different Pulse Selectors Using FEA-Based Model

AHMED NASR [1], **CHUNYANG GU** [2] (Senior Member, IEEE), **JING LI** [1] (Senior Member, IEEE),
GIAMPAOLO BUTICCHI [1] (Senior Member, IEEE), **SALMAN IJAZ** [1],
CHRIS GERADA [3] (Senior Member, IEEE), AND **HE ZHANG** [1] (Senior Member, IEEE)

[1]Key Laboratory of More Electric Aircraft Technology of Zhejiang Province, University of Nottingham Ningbo China, Ningbo 315100, China
[2]Advanced Electrical Machine Drive Research Center, Yongjiang Laboratory, Ningbo 315202, China
[3]Power Electronics, Machines, and Control Research Group, University of Nottingham, NG7 2RD Nottingham, U.K.

CORRESPONDING AUTHOR: JING LI (e-mail: jing.li@nottingham.edu.cn)

ABSTRACT Despite the robustness and fast dynamic response, direct torque control (DTC) exhibits relatively large ripples in torque and flux during steady-state operation. Mitigating these ripples depends on designing a pulse selector to identify the optimal voltage vector at every control cycle, which has been reported with different structures in the literature. Hence, it is becoming increasingly crucial to comprehensively understand the criteria used in pulse selection and analyze their impact on the overall DTC performance. These are challenging in permanent magnet synchronous motor (PMSM) drives due to the nonlinear torque/current characteristics and spatial harmonics of the magnetic flux. This article exploits the high fidelity and computational efficiency of the finite-element analysis (FEA)-based model to present a performance prediction strategy for DTC of PMSM under different pulse selectors. First, this model is employed to thoroughly analyze the influence of each switching pulse on the torque and flux deviations under changing operating conditions considering the machine's nonlinearities. Then, the pulse selection schemes used in switching-table-based DTC are comparatively evaluated, highlighting the advantages and limitations of each. Based on this evaluation, an advanced pulse selector with a variable-structure switching table (VSST) is developed, reducing torque/flux ripples and simplifying the control implementation while maintaining the fast dynamic response of DTC.

INDEX TERMS Direct torque control (DTC), finite-element analysis (FEA), permanent magnet synchronous motor (PMSM), pulse selection, torque ripple.

I. INTRODUCTION

Due to their high efficiency, power density, and wide speed range, permanent magnet synchronous motors (PMSMs) are widely utilized in several applications, including electrified transportation, robotics, and renewable energy systems [1], [2]. The high-performance requirements of these applications imply the necessity for employing a robust and reliable control technique. Direct torque control (DTC) has gained considerable attention since it was first implemented on PMSM drives

by Zhong et al [3] in 1997 owing to its fast dynamic response, insensitivity to rotor parameter variation, and inherently sensorless nature [4]. It achieves these control features by directly manipulating the voltage vector applied to the machine winding using a pulse selector. This vector drives the stator flux vector in the direction that satisfies the demanded variation in torque and stator flux amplitude [5]. Hence, the pulse selector is a key component in DTC that has a significant impact on the drive performance.

The basic principle of the pulse selector is to use a look-up table to set the switching states of the inverter depending on rough estimation of the stator-flux angular position and indication of the demanded deviation direction in torque and flux using two hysteresis regulators. The selected switching pulse is applied for the entire control cycle, ensuring almost the theoretical maximum dynamic performance. However, this leads to pronounced torque and flux ripples during steady-state operation, especially in the case of two-level inverters [6], [7]. Torque tracking with minimum steady-state ripples can avoid the acoustic noise and vibration that cause wear and tear of the mechanical components (such as the shaft, bearings, and loads) [8]. To minimize the torque and flux ripples, many researchers have attempted to improve the criteria used in pulse selection.

In [9], [10], [11], [12], [13], the look-up table structure is modified in terms of either the included switching positions (i.e., the admitted voltage vectors), the number of levels for the torque hysteresis regulator, or the sector definition needed to indicate the stator-flux angular position. Furthermore, duty-ratio regulators have been employed in [14], [15], [16], [17], [18] to apply two or more voltage vectors at every control period during steady-state operation. Although these modifications can effectively reduce the torque ripple, they introduce other performance issues, such as increased flux ripple and current harmonics, and complicated control implementation (by introducing additional control parameters).

Other researchers attempted to ensure selecting the optimal switching pulse that reduces both the torque and flux ripple using the model predictive control (MPC) solution [19], [20]. MPC uses the machine model to predict the torque and flux trajectories under all admissible voltage vectors, and the optimal options are selected based on a cost-function evaluation. However, the need for the predictions and the weighting factor to tune the importance of each control objective increases the computational complexity and degrades the DTC robustness [21]. The need for a weighting factor can be eliminated using sequential and parallel optimization strategies, as presented in [22], [23], [24]. The cost function of each control objective are separately considered. From the point of view of each cost function, the admissible switching pulses are ranked in groups of a predefined number of candidates, from which the optimal option is selected. Moreover, the computation complexity of MPC can be reduced by artificially preselecting the candidate switching states before the prediction phase, as described in [25], [26], [27]. Despite the ability of these methods to optimize the switching pulses selection, they fails to identify the pulse patterns that minimize the flux ripple and current harmonics [28].

Alternatively, a space vector modulator (SVM) has been utilized in [29] to synthesize the exact voltage vector that accurately satisfies the required deviations in torque and flux. This voltage vector is identified from the demanded stator flux vector, the angular position of which is derived from the desired torque deviation via a proportional-integral (PI) controller. To avoid degradation of the DTC dynamic performance, a deadbeat (DB) controller replaces the PI regulator in [30], where the demanded stator-flux vector is determined using the machine model. In [31], the computation complexity of the DB controller has been reduced by directly deriving the reference voltage vector from the torque error. Instead, a sliding mode controller (SMC) is employed in [32], which can handle the unknown disturbances and modeling inaccuracies. Nevertheless, compared to the switching look-up table DTC, the use of a SVM complicates the control implementation and results in a higher switching frequency which is undesired in medium- and high-voltage drives [33].

With the wide variety of criteria used for pulse selection in DTC and the corresponding objectives, it is becoming increasingly crucial to comprehensively analyze their impact on control performance. A machine model with several simplifying assumptions has been employed in the aforementioned literature (such as [15], [16], [18], [26], [27]) to investigate the effect of each switching pulse on the torque and flux modulus, then to predict the control performance under the presented pulse selector. This model fails to accurately represent the dynamic behavior of PMSM because of the nonlinear torque-current characteristics and rotor position-dependent variation in the magnetic energy that results in flux harmonics and cogging effects [34]. These inaccuracies can seriously compromise the prediction quality of the PMSM-drive control performance. Therefore, accurate model-based analysis for the pulse selection criteria, can be useful during the control design to thoroughly evaluate the control behavior. Among the competing high-fidelity modeling techniques of PMSM [34], [35], [36], [37], [38], the finite-element analysis (FEA)-based model in synchronous rotating coordinates (dq), can provide the highest computational efficiency while considering various non-ideal characteristics, such as magnetic saturation, iron losses, and spatial harmonics.

Therefore, this article proposes a detailed performance analysis for the pulse selection criteria in DTC of PMSM drives using the FEA-based model. It addresses different structures of the pulse selectors, including their basic principles, control objectives, and factors that cause control performance issues. The main contribution of the current work can be summarized as follows:

- The FEA-based PMSM model is used to theoretically investigate the effects of each switching pulse admitted by the converter on the torque and flux responses under different operating conditions considering the magnetic saturation of the machine. From the perspective of this investigation, different pulse selectors are comparatively evaluated by highlighting the main features and limitations of each.
- To overcome these limitations, a variable-structure-switching table (VSST)-based strategy is proposed for pulse selection in DTC. This method not only ensures reduced torque and flux ripples but also simplifies the control implementation and reduces the average

switching frequency while maintaining the fast dynamic response.

- By synthesizing the voltage vectors selected by the DTC schemes via the converter switching function, the FEA-based model is exploited to obtain a fast and high-fidelity prediction for the performance of the PMSM drive system.

Simulations in Matlab/Simulink via the FEA-based PMSM model is compared with those obtained by the simplified model to verify the feasibility of the proposed performance prediction strategy. Then, experimental evaluations for different DTC pulse selectors are performed on a laboratory prototype of a PMSM drive system to verify the effectiveness of the proposed pulse selection technique with the VSST.

The rest of this article is organized as follows. Section II describes the basic principle of different pulse selectors used in DTC scheme. In Section III, the FEA-based PMSM model is used to analyze these pulse selectors, and the performance prediction strategy is demonstrated. Then, an advanced VSST-based pulse selection method is proposed in Section IV. To validate the outcomes of the performance analysis, simulation results are discussed in Section V. After that, experimental verification of the proposed VSST-based method is presented in Section VI. Finally, conclusions are drawn in Section VII.

II. PULSE SELECTION IN DTC OF PMSM

A. PRINCIPLE OF DTC

The dynamic behavior of the DTC's controlled variables (i.e., torque and flux) depends on the voltage vector applied to the machine terminals, which can be represented by different mathematical models for PMSM [37]. If the flux-linkage-based model in the stationary coordinates ($\alpha\beta$) is employed, the stator flux vector ($\boldsymbol{\psi}_{\alpha\beta} = \psi_\alpha + \mathrm{j}\psi_\beta$) and the electromagnetic torque (T_e) can be expressed as

$$\boldsymbol{\psi}_{\alpha\beta} = \int \left(\mathbf{v}_{\alpha\beta} - R_s \mathbf{i}_{\alpha\beta} \right) \mathrm{d}t \tag{1}$$

$$T_e = \frac{3p}{2} \left(\boldsymbol{\psi}_{\alpha\beta} \times \mathbf{i}_{\alpha\beta} \right), \tag{2}$$

where $\mathbf{v}_{\alpha\beta}$ and $\mathbf{i}_{\alpha\beta}$ are the stator voltage and current vectors, respectively, R_s represents the stator phase resistance, and p denotes the number of pole pairs. From (1), when DTC applies an arbitrary voltage vector $\mathbf{v}_{\alpha\beta}^*$ to the stator winding for a sampling period T_s, it deviates the stator flux vector by $\Delta\boldsymbol{\psi}_{\alpha\beta} = \mathbf{v}_{\alpha\beta}^* T_s$ (assuming that R_s is negligible). This deviation adjusts the amplitude ($\psi_s = \|\boldsymbol{\psi}_{\alpha\beta}\|$) and angular position ($\theta_s = \arctan(\psi_\beta/\psi_\alpha)$) of the stator flux vector. By adjusting θ_s, the (load) angle between the stator and rotor flux vectors can be directly manipulated due to the fast dynamics of the stator flux compared to that of the machine rotor [3].

To illustrate the effect of the direct manipulation of the load angle on the torque, (2) needs to be simplified by neglecting the magnetic saturation effects (i.e., the stator inductance L_s is constant). As a result, the stator current vector can be written
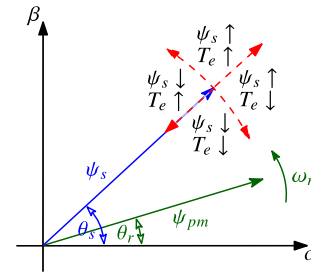

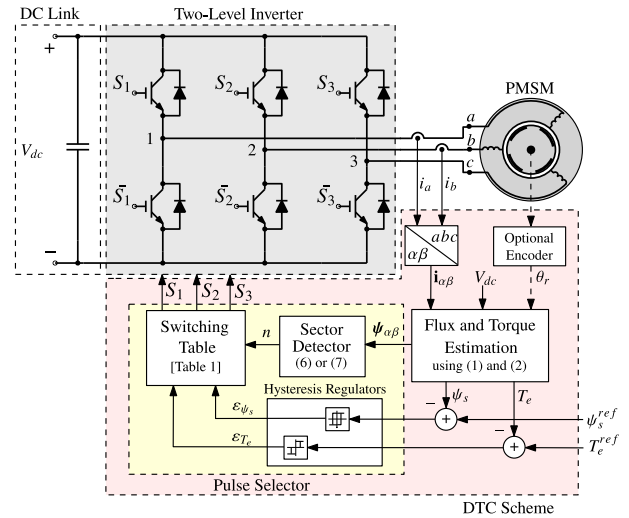**FIGURE 1.** Illustration of the DTC basic principle.

FIGURE 2. Block diagram of DTC scheme for PMSM drive system.

as

$$\mathbf{i}_{\alpha\beta} = \frac{1}{L_s} \left(\boldsymbol{\psi}_{\alpha\beta} - \psi_{pm} e^{\mathrm{j}\theta_r} \right), \tag{3}$$

where ψ_{pm} is the permanent magnet flux, and θ_r is the rotor angular position. Substituting (3) into (2), the torque equation can be rewritten as

$$T_e = \frac{3p\psi_s\psi_{pm}}{2L_s} \sin\left(\theta_s - \theta_r\right). \tag{4}$$

This implies that increasing or decreasing the load angle (i.e., $(\theta_s - \theta_r)$) can increase ↑ or decrease ↓ the torque if the stator flux amplitude ψ_s is maintained constant. Consequently, the direct control of torque and stator flux amplitude is accomplished by controlling the stator flux vector along its tangential and radial directions, as illustrated by Fig. 1. Thus, the proper selection of the voltage vector applied to the stator winding is the key to providing optimal control performance.

B. CRITERIA USED IN PULSE SELECTION

Aiming at robustness against parameter variation and fast dynamic response, the DTC employs a pulse selector to set a basic voltage vector among those admitted by the power converter, as shown in Fig. 2. With a two-level voltage source inverter, only eight basic voltage vectors ($\mathbf{v}_{\alpha\beta}[x]$) are feasible
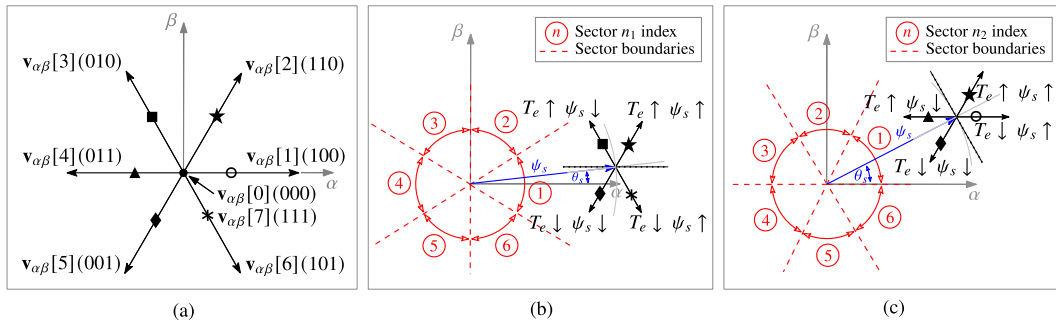
FIGURE 3. Illustration of the feasible voltage vectors with the corresponding switching pulses $\mathbf{v}_{\alpha\beta}[x](S_1 S_2 S_3)$ (a) and their influence on the torque T_e and stator flux amplitude ψ_s when the stator flux vector is located in Sector ① with the sector definition n_1 (b) and n_2 (c).

according to the switching pulses $(S_1 S_2 S_3)$, the space vectors of which can be written as

$$\mathbf{v}_{\alpha\beta}[x] = \frac{2}{3} V_{dc} \left(S_1[x] + S_2[x] e^{j\frac{2\pi}{3}} + S_3[x] e^{j\frac{4\pi}{3}} \right), \quad (5)$$

where $x \in \{0, 1.., 7\}$ is the voltage-vector index. Two of these voltage vectors ($x \in \{0, 7\}$) are zero voltage vectors (ZVVs), and the others are active voltage vectors (AVVs), which are defined in Fig. 3(a). By considering the influence of each vector on the deviation direction of the stator flux vector, the most feasible option can be properly selected.

Because this effect relies on the angular position of the stator flux vector θ_s, the $\alpha\beta$-plane is typically divided into six sectors ($n \in \{1, 2.., 6\}$) with two different boundary definitions n_1 and n_2, as shown in Fig. 3(b) and (c). Therefore, a sector detector is employed to identify that position using one of the following expressions:

$$Sector\ n_1 : \quad \frac{(2n_1 - 3)\pi}{6} < \theta_s \leq \frac{(2n_1 - 1)\pi}{6} \quad (6)$$

$$Sector\ n_2 : \quad \frac{(2n_2 - 2)\pi}{6} < \theta_s \leq \frac{2n_2\pi}{6} \quad (7)$$

For both sector definitions, Fig. 3(b) and (c) give an illustration of the influence of the voltage vectors on the torque T_e and stator flux amplitude ψ_s when the stator flux vector is located in Sector $n = 1$. The ZVV's (●) effects on torque and flux are considered negligible. The AVV indexed $x = 2$ (★) and $x = 5$ (◆) respectively increases and decreases both T_e and ψ_s. With the sector definition n_1, the vector $x = 3$ (■) increases T_e and decreases ψ_s, and vice versa for $x = 6$ (✳). These two vectors are replaced in the sector definition n_2 with those indexed $x = 4$ (▲) and $x = 1$ (○) to satisfy a more pronounced impact on ψ_s. As the phase shift between the voltage vectors matches the spatial range of the sectors (i.e., $\pi/3$), these impacts of the AVVs indexed as 2, 5, 3, 6, 4, and 1 will be respectively similar to those of 3, 6, 4, 1, 5, and 2 when the stator flux vector is located in Sector $n = 2$. Thus, the voltage vector index x can be expressed using the sector identifiers to generalize the description of their influence on
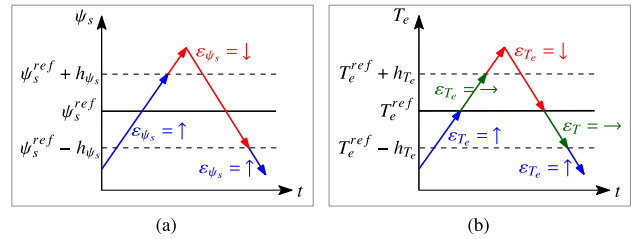
FIGURE 4. Hysteresis regulators of stator flux amplitude (a) and torque (b) used in DTC.

the controlled variables as follows.

$$If\ x = \begin{cases} n_1 + 1\ or\ n_2 + 1, & then\ T_e \uparrow \psi_s \uparrow \\ n_1 + 2\ or\ n_2 + 3, & then\ T_e \uparrow \psi_s \downarrow \\ n_1 + 5\ or\ n_2, & then\ T_e \downarrow \psi_s \uparrow \\ n_1 + 4\ or\ n_2 + 4, & then\ T_e \downarrow \psi_s \downarrow \end{cases} \quad (8)$$

where the voltage index $x = x - 6$, if $x > 6$.

As the DTC chooses the switching pulses of the voltage vector to force the torque and flux magnitude to track their reference signals T_e^{ref} and ψ_s^{ref}, two- or three-level hysteresis regulators are used to indicate the demanded deviation direction (ε_{ψ_s} and ε_{T_e}), such that $\uparrow$, $\rightarrow$, and $\downarrow$ represent the three possible directions. ε_{ψ_s} and ε_{T_e} are obtained based on the error between the estimated and reference values and the hysteresis bands ($\pm h_{\psi_s}$ and $\pm h_{T_e}$), as depicted in Fig. 4. According to the output of the hysteresis regulators and the indicated sector n, the index of the most feasible voltage vector can be chosen from a look-up table among those shown in Table 1.

Four different look-up tables are presented in Table 1 [3], [9], [10], [11]. The basic switching table (BST) and the modified BST (MBST) use a three-level hysteresis torque regulator and employ the ZVVs when the torque needs to be maintained constant ($\varepsilon_{T_e} = \rightarrow$). Unlike the other switching tables, MBST uses (7) instead of (6) to detect the sector n. Thus, it uses the AVVs indexed $[n+3]$ and $[n]$ rather than $[n+2]$ and $[n+5]$ to respectively increase and decrease the torque. Table 1(c) and (d) exclude one torque state ($\varepsilon_{T_e} = \rightarrow$) by using two-level hysteresis regulator. The former employs the AVVs only, while the other utilizes the ZVVs when both the torque and the flux

TABLE 1. Different Switching Look-Up Tables for DTC

(a) Basic switching table (BST)

ε_{ψ_s} \ ε_{T_e}	↑	→	↓
↑	n+1	0,7	n+5
↓	n+2	0,7	n+4

$n = n_1$ is detected using (6)

(b) Modified BST (MBST)

ε_{ψ_s} \ ε_{T_e}	↑	→	↓
↑	n+1	0,7	n
↓	n+3	0,7	n+4

$n = n_2$ is detected using (7)

(c) AVVs switching table (AST)

ε_{ψ_s} \ ε_{T_e}	↑	↓
↑	n+1	n+5
↓	n+2	n+4

$n = n_1$ is detected using (6)

(d) ZVV switching table (ZST)

ε_{ψ_s} \ ε_{T_e}	↑	↓
↑	n+1	n+5
↓	n+2	0,7

$n = n_1$ is detected using (6)

modulus has to be decreased (i.e., $\varepsilon_{T_e} = \downarrow$ and $\varepsilon_{\psi_s} = \downarrow$). For convenience, these switching tables are respectively specified in this work as AST and ZST.

Accordingly, the criteria used for pulse selection in DTC can change the control performance by considering a number of factors that can be summarized as follows:

1) The sector definition used to indicate the location of the stator voltage vector in the $\alpha\beta$ plane.
2) The number of levels of the hysteresis regulators and the width of hysteresis bands.
3) The structure of the switching look-up table and the included voltage vectors.

For setting these criteria, only the influence of the switching pulses on the stator flux vector has been considered in the conventional DTC by assuming that it depends only on the direction of the corresponding voltage vectors. However, by thoroughly analyzing these influences under different operating conditions (such as the rotor speed and the load torque), the criteria used for pulse selection in DTC can be better set, improving the overall control performance. To achieve that, a performance prediction strategy for the DTC is presented in the following section.

III. PERFORMANCE PREDICTION OF DTC

The impact of the switching pulses on the torque and flux responses can be principally predicted based on the PMSM model, which has been represented mathematically by simplified or FEA-based models. In this section, predictions for the torque and flux responses of PMSM using both models are presented first. Then, the pulse selectors presented in Section II are analyzed under different operating conditions to predict the DTC performance, highlighting the advantages and disadvantages of each.

A. SIMPLIFIED PREDICTION OF TORQUE AND FLUX RESPONSES

To simplify the prediction of the torque and flux responses, various assumptions have been considered for the PMSM model (3) and (4), [14], [15], [16], [17], [18], [27]. For instance, the rotor saliency is ignored, the hysteresis and saturation properties of the magnetic core are neglected, and the permanent magnet flux (ψ_{pm}) is assumed to be sinusoidally distributed in the air gap and aligned with the d-axis direction. As a result, the magnetic saturation and flux harmonics caused by the magnetic energy variation with the rotor position are ignored. The d- and q-axis components of the stator inductance (L_d and L_q) have been dealt as equivalent and constant values (i.e., $L_d = L_q = L_s$).

Consequently, the variations of torque and stator flux magnitude over the sampling period T_s due to applying the voltage vector $\mathbf{v}_{\alpha\beta}[x]$ can be derived from (1)–(3) as [15]:

$$\Delta T_e[x] = \frac{3pT_s}{2L_s}\left(\boldsymbol{\psi}_r \times \mathbf{v}_{\alpha\beta}[x] - \frac{R_s}{L_s}\left(\boldsymbol{\psi}_r \times \boldsymbol{\psi}_{\alpha\beta}\right)\right.$$
$$\left. - \boldsymbol{\psi}_{\alpha\beta} \times j\omega_r\boldsymbol{\psi}_r\right), \tag{9}$$

$$\Delta\psi_s[x] = \frac{T_s}{\psi_s}\left(\boldsymbol{\psi}_{\alpha\beta}\cdot\mathbf{v}_{\alpha\beta}[x] - \frac{R_s}{L_s}\left(\psi_s{}^2 - \boldsymbol{\psi}_{\alpha\beta}\cdot\boldsymbol{\psi}_r\right)\right), \tag{10}$$
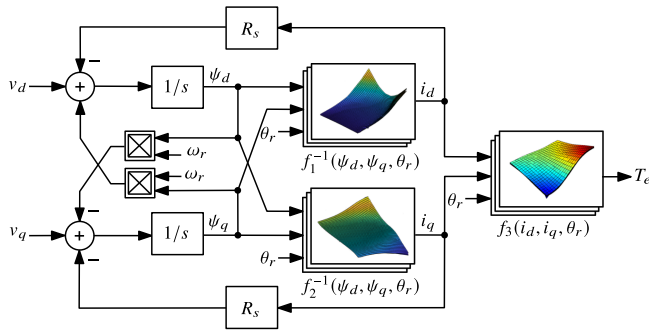
where $\boldsymbol{\psi}_r = \psi_{pm}e^{j\theta_r}$. Usage of (9) and (10) to predict the impact of the switching pulses on the torque and flux amplitude responses provides acceptable accuracy for the surface-mounted PMSM (SPMSM) owing to its non-salient rotor and the relatively large air gap between the stator and rotor cores. However, with the above-mentioned assumptions, these expressions can seriously compromise the prediction quality of the control performance for the interior PMSM (IPMSM) because of the rotor saliency that not only introduces nonlinear torque-current characteristics but also causes a rotor position-dependent variation of the magnetic energy, leading to flux harmonics and cogging effects [39]. To overcome this issue, a fast and accurate PMSM model is needed for the performance prediction of DTC. Although the FEA can satisfy the required accuracy, it is computationally time-consuming. Reducing the calculation time significantly is feasible by pre-calculating and storing the FEA results for offline processing. Thus, the FEA-based PMSM model [34] can be a promising solution to predict the DTC performance.

B. PROPOSED PERFORMANCE PREDICTION STRATEGY USING FEA-BASED MODEL

The FEA-based model can capture the nonlinear characteristics of PMSM by extracting the d- and q-components of the stator flux (ψ_d and ψ_q) and the torque from FEA at different values of d- and q-axis currents (i_d and i_q) and rotor angular position θ_r. To ensure the computational efficiency of this modeling scheme, the extracted data can be represented by either curve fitting or lookup tables as

$$\begin{cases} \psi_d = f_1\left(i_d, i_q, \theta_r\right) \\ \psi_q = f_2\left(i_d, i_q, \theta_r\right), \end{cases} \tag{11}$$

$$T_e = f_3\left(i_d, i_q, \theta_r\right). \tag{12}$$

FIGURE 5. Schematic representation of the FEA-based PMSM model.

FIGURE 6. Polar representation of the torque deviation ΔT_e (N · m) produced by $\mathbf{v}_{\alpha\beta}[x = 1]$ with the angular position of stator-flux vector θ_s (rad) under different loading conditions and operating speeds. (a) at 300 r/min. (b) at 3000 r/min. [Solid line: using FEA-based model; Dashed line: using simplified model].

In this model, the rotating frame (dq) representation of the machine variables (i.e., stator flux, current, voltage) reduces the amount of data need to be extracted from FEA [36]. As these variables can be obtained from their $\alpha\beta$ presentation using Park's transform ($\mathbf{f}_{dq} = \mathbf{f}_{\alpha\beta}e^{-j\theta_r}$), the stator flux equation (1) is rewritten as:

$$\boldsymbol{\psi}_{dq} = \int \left(\mathbf{v}_{dq} - R_s\mathbf{i}_{dq} - j\omega_r\boldsymbol{\psi}_{dq} \right) dt, \tag{13}$$

where $\omega_r = d\theta_r/dt$ denotes the rotor angular speed, and $\mathbf{v}_{dq}$ is the applied voltage vector that can be obtained from (5) as $\mathbf{v}_{\alpha\beta}e^{-j\theta_r}$. According to (13), the impact of the voltage vector on the stator flux can be predicted if the dq components of the stator-current vector $\mathbf{i}_{dq}$ are obtained as functions of the corresponding flux linkages and the rotor position as

$$\begin{cases} i_d = f_1^{-1}\left(\psi_d, \psi_q, \theta_r\right) \\ i_q = f_2^{-1}\left(\psi_d, \psi_q, \theta_r\right). \end{cases} \tag{14}$$
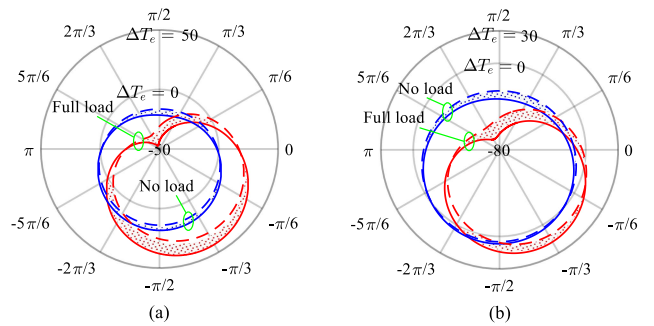
A data set for these functions can be obtained by inverting (11) using, for example, MATLAB's gridfit function [40]. Based on (12)–(14), the schematic representation of the FEA-based PMSM model can be illustrated by Fig. 5. The implementation and verification steps for the FEA-based model of the 80-kW PMSM prototype under study, with the parameters given in the Appendix, are well described in [41] and not repeated here for the sake of space.

If a voltage vector $\mathbf{v}_{dq}[x] = v_d[x] + jv_q[x]$ is applied at the kth control sample, the d- and q-axis flux linkages can be predicted from the discrete form of (13) as

$$\begin{cases} \psi_d^{k+1}[x] = \psi_d^k + T_s\left(v_d^k[x] - R_si_d^k - \omega_r^k\psi_q^k\right) \\ \psi_q^{k+1}[x] = \psi_q^k + T_s\left(v_q^k[x] - R_si_q^k + \omega_r^k\psi_d^k\right), \end{cases} \tag{15}$$

where ψ_d^k and ψ_q^k are determined from (11) according to the loading condition represented by the currents i_d^k and i_q^k. Based on (15), the d- and q-components of the current vector at the sampling instant $k + 1$ can be predicted using (14), and the deviations in torque and stator-flux modulus can be obtained for each admissible voltage vector x as

$$\Delta T_e[x] = f_3\left(i_d^{k+1}[x], i_q^{k+1}[x], \theta_r^{k+1}\right) - f_3\left(i_d^k, i_q^k, \theta_r^k\right), \tag{16}$$

$$\Delta\psi_s[x] = \sqrt{(\psi_d^{k+1}[x])^2 + (\psi_q^{k+1}[x])^2} - \sqrt{(\psi_d^k)^2 + (\psi_q^k)^2}, \tag{17}$$

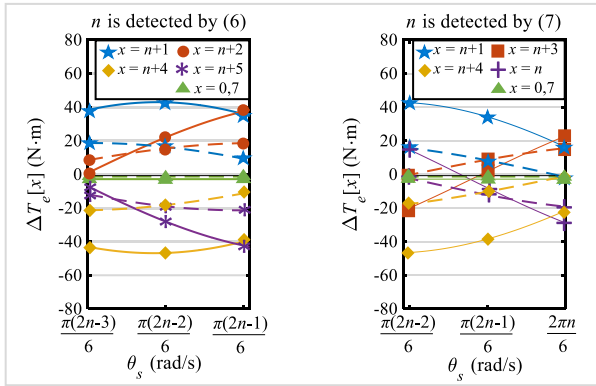where $\theta_r^{k+1} = \theta_r^k + \omega_r^kT_s$. In this way, the impact of the voltage vector on the torque and flux-amplitude responses can be analyzed using the FEA data instead of the simplified model, resulting in more accurate predictions for the DTC control performance.

To illustrate, ΔT_e produced by $\mathbf{v}_{\alpha\beta}[x = 1]$ throughout the whole spatial range of θ_s under different operating conditions is calculated using the simplified and FEA-based models of the 80-kW PMSM prototype, as shown in Fig. 6. For these computations, the sampling interval T_s is set to 50 μs, and only the magnetic saturation is considered (i.e., θ_r is maintained zero in (11)–(14)). From Fig. 6, it can be seen that the simplified model exhibits lower absolute torque deviations than the FEA-based model over a wide range of θ_s under all operating conditions [see the dotted areas in Fig. 6]. Consequently, if the former is employed to assess the torque control performance of DTC strategies, it will show lower torque ripple and slower dynamic response, as will be confirmed in Section V. Thus, the FEA-based model is employed to evaluate the DTC performance under different pulse selectors as follows.
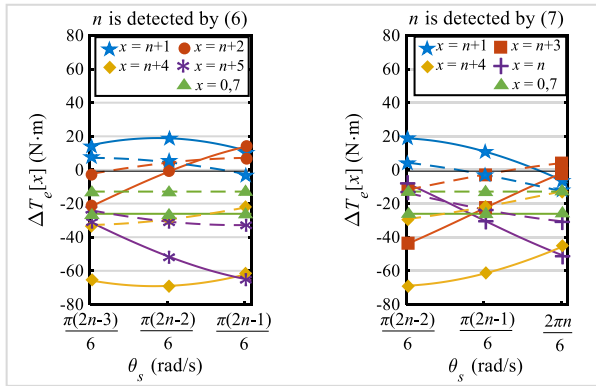
C. COMPARATIVE ANALYSIS OF PULSE SELECTION CRITERIA USING FEA-BASED MODEL

The criteria used in pulse selection of DTC are theoretically analyzed using the FEA-based model considering only the magnetic saturation. The torque and flux variations generated by each voltage vector included in the switching tables [see Table 1] are calculated using (16) and (17) at a control sample of $T_s = 50$ μs. These deviations are determined at different operating conditions over the entire spatial range of both sector definitions (6) and (7), as shown in Figs. 7 and 8.
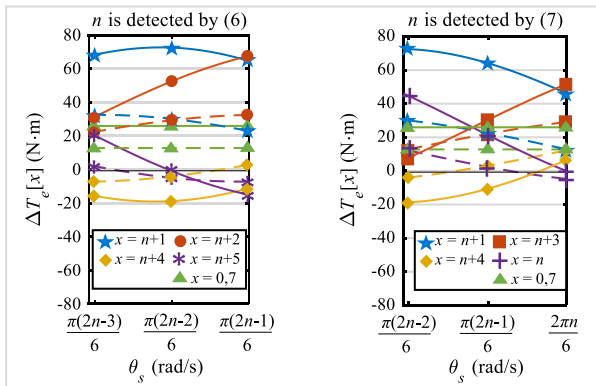
As can be noticed from Figs. 7 and 8, the voltage vectors employed with the sector definition (7) produce lower torque deviations and higher flux variations than those used with (6), regardless the operating conditions. Consequently, employing
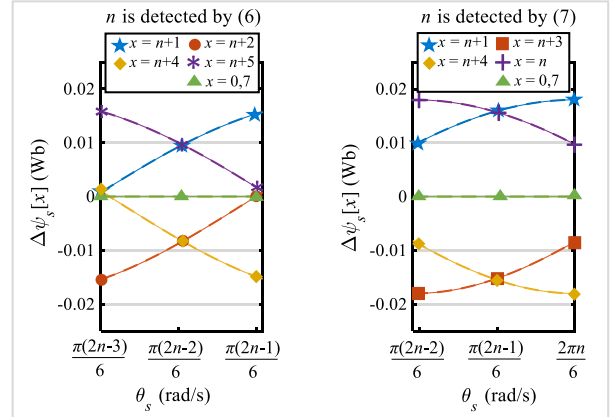
(a) At 100 r/min

(b) At +3000 r/min

(c) At -3000 r/min

FIGURE 7. Torque deviation ΔT_e produced by each voltage vector included in the switching tables [Table 1] when applied for a control period of $T_s =$ 50 μs within the spatial range of sector n at different operating conditions. [Solid line: at 80% of full load; Dashed line: at no load].

FIGURE 8. Stator-flux amplitude deviation $\Delta \psi_s$ produced by each voltage vector included in the switching tables [Table 1] when applied for a control period of $T_s =$ 50 μs within the spatial range of sector n.

strengthen. Thus, the torque decay will be faster than the torque rise for all pulse selectors. Also, both voltage vectors [$n+3$] and [n] fails to respectively increase and decrease the torque at high-speed ($\pm$3000 r/min) and loading conditions, which can result in failure of MBST to maintain stable operation, as will be confirmed in Sections V and VI.

From Fig. 7(b) and (c), the ZVV produces torque deviations that are always in a direction opposite to that of the rotation. These deviations are lower than those developed by [$n+4$] and [$n+5$] for positive speed and [$n+1$] and [$n+2$] for negative speed. Consequently, ZST can provide reduced torque ripple compared to AST, as the former utilizes the ZVVs at one of the table states. However, applying a ZVV at that state results in a slower torque response when a torque decay is demanded. Also, ZST cannot allow speed reversal as the torque deviation produced by ZVV becomes positive when the rotation direction changes, i.e., the ZVV fails to satisfy the condition $\varepsilon_{T_e} =\downarrow$ in ZST. Therefore, a voltage-vector selection strategy based on a variable-structure switching table is presented in the following section.

IV. PROPOSED PULSE SELECTION STRATEGY WITH A VARIABLE-STRUCTURE SWITCHING TABLE (VSST)

As discussed in Section III-C, the torque and flux deviations depend not only on the angular position of the stator-flux vector but also the operating conditions, such as the direction of rotation. Hence, selecting the switching pulse from a look-up table with a changing structure based on these conditions can be a desired feature from the point of view of steady-state and dynamic performances of DTC.

The proposed strategy detects the sector n using (6) to avoid the performance issues associated with MBST at high speeds. When the motor speed is positive, applying a ZVV to decrease the torque ($\varepsilon_T =\downarrow$) instead of the AVVs [$n+4$] or [$n+5$] can improve the steady-state performance in terms of the torque and flux ripples because of two reasons. The

MBST for DTC of PMSM can cause lower torque ripple, slower dynamic response, and higher flux ripple compared to the other switching tables (BST, AST, and ZST).

By comparing Fig. 7(b) with Fig. 7(a), it can be noted that, with the speed increase in the anticlockwise direction (+ve speed), the positive torque deviations produced by either the AVVs [$n+1$], [$n+2$], or [$n+3$] weaken, while the negative torque deviations generated by [$n+4$], [$n+5$], or [n]

TABLE 2. Proposed Variable-Structure Switching Table (VSST)

Error Signals of Torque and Flux		Steady State		Dynamic State
T_{err}	ψ_{err}	↻	↺	
$T_{err} \geq 0$	$\psi_{err} \geq 0$	$n+1$	$0,7$	$n+1$
	$\psi_{err} < 0$	$n+2$	$0,7$	$n+2$
$T_{err} < 0$	$\psi_{err} \geq 0$	$0,7$	$n+5$	$n+5$
	$\psi_{err} < 0$	$0,7$	$n+4$	$n+4$

n is detected using (6).

↻ and ↺ are rotation directions.

FIGURE 9. Flowchart of the proposed pulse selection strategy with VSST.

ZVVs produce lower negative torque deviations [see Fig. 7(a)] and their impact on the flux is negligible [see Fig. 8]. The steady-state-performance improvement can be maintained in the backward direction of rotation (i.e., −ve speed) by employing ZVVs to increase the torque (when $\varepsilon_T = \uparrow$) instead of the AVVs [$n+1$] or [$n+2$]. The ZVV is decided (0 or 7) to minimize the number of switching jumps, such that $\mathbf{v}_{\alpha\beta}[0]$ follows the voltage vectors indexed as 0, 1, 3, and 5, while the remaining vectors are followed by $\mathbf{v}_{\alpha\beta}[7]$. Because the ZVVs degrade the dynamic performance if a decay in the absolute torque is demanded, the AVVs are the best option at all the table states (as in the case of AST). Hence, the proposed strategy uses the variable-structure switching table (VSST) shown in Table 2, where the voltage vector index needs to be artificially selected considering the operating state and the rotation direction.

To achieve that, a simple strategy can be utilized for pulse selection, which is illustrated by the flowchart shown in Fig 9.

The dynamic state of the system can be activated by detecting the demanded-torque transition (ΔT_e^{ref}). To guarantee the speed reversal, the activation of the dynamic state has to be maintained using a "$flag$" till the satisfaction of two conditions: (1) The estimated torque crosses the reference signal (i.e., $\text{sgn}(T_{err}^k) \neq \text{sgn}(T_{err}^{k-1})$); (2) The direction of rotation is similar to that of the reference torque ($T_e^{ref} \cdot \omega_r^k \geq 0$).

According to the VSST [Table 2], one of two AVVs will be applied during steady-state conditions depending on the rotational direction ([$n+1$] or [$n+2$] for clockwise and [$n+5$] or [$n+4$] for anticlockwise). As can be noticed in Fig. 8, the absolute flux deviations produced by [$n+2$] and [$n+5$] are significantly higher than those generated by [$n+1$] and [$n+4$], respectively, when θ_s is in the range of the *Subsector* I $\in [(2n-3)\pi/6, \ (2n-3)\pi/6 + \pi/12)$. Conversely, the AVVs [$n+1$] and [$n+4$] give higher absolute flux deviations when θ_s is in the range of the *Subsector* II $\in ((2n-1)\pi/6 - \pi/12, \ (2n-1)\pi/6]$. As a result, the switching between the two possible AVVs during the transition from one sector to another leads to a considerable change in the stator flux amplitude, degrading the flux control performance. To avoid this issue, the vector index selected from VSST needs to be replaced according to the conditions shown in Fig. 9. The pulse replacement not only alleviates the occasional compromise
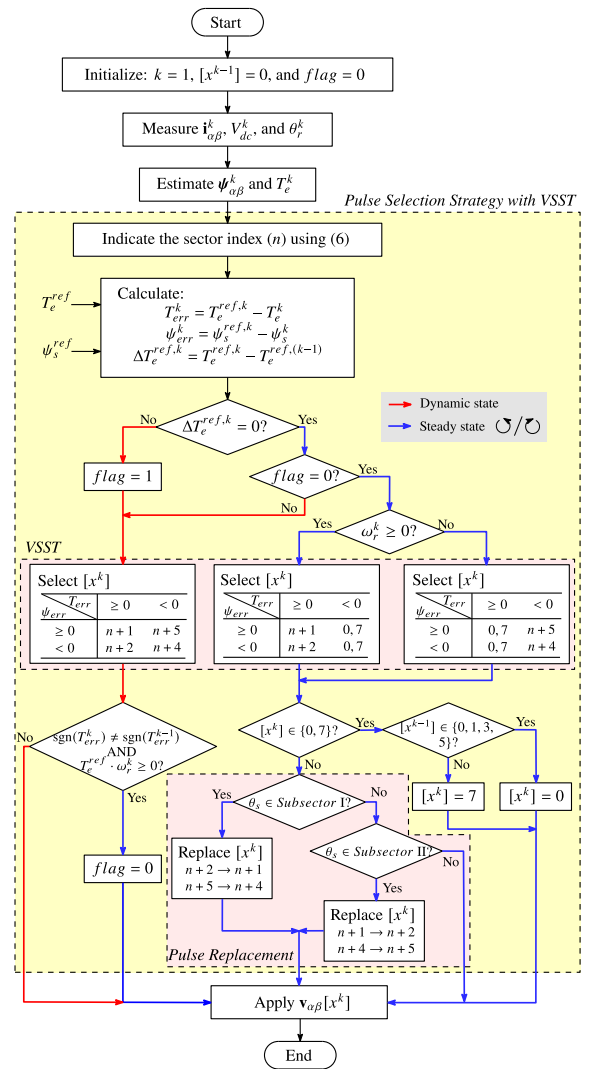
of the flux regulation but also avoids the undesired torque-deviation directions produced by the replaced voltage vectors at high-speed conditions.
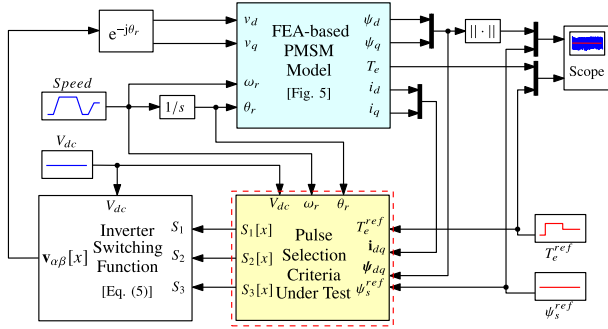
With this simple strategy, the switching-table structure is made variable depending on the operating state and direction of rotation, achieving improved steady-state torque performance while retaining the classical methods' fast dynamic response and robustness. Moreover, the control implementation is simplified by using the sign of the torque and flux error ($T_{err} = T_e^{ref} - T_e$ and $\psi_{err} = \psi_s^{ref} - \psi_s$) instead of the hysteresis regulators and the corresponding tuning of their band limits. As will be discussed in the following sections, the simulations and experimental results confirm the effectiveness of the proposed strategy.

V. SIMULATION RESULTS
A. SYSTEM DESCRIPTION AND SIMULATION PARAMETERS
The PMSM drive system shown in Fig. 10 is used to predict the DTC performance under different pulse selectors to verify

FIGURE 10. FEA-based PMSM drive system for performance prediction of DTC.

FIGURE 11. Simulation results of the steady-state performance at no load and different speeds. (a) At 100 r/min. (b) At 3000 r/min. [from top to bottom: torque T_e, stator-flux modulus ψ_s, and average switching frequency f_{av}].

the theoretical analysis discussed in Section III-C, and validate the effectiveness of the proposed pulse selection strategy presented in Section IV. The PMSM is driven in torque control mode where the operating speed (ω_r) is controlled via a virtual dynamometer, from which the rotor angular position θ_r can be indicated. The machine states (i.e., flux and torque) are given to the pulse selector of DTC to decide the stator voltage that forces them to follow the predefined reference signals. By using (5), the stator voltage can be fed to the FEA-based model [Fig. 5] to predict the torque and flux control performances in terms of steady-state ripples and average switching frequency (f_{av}). The torque and flux ripples can be represented using the standard deviation (σ_{T_e} and σ_{ψ_s}), as

$$\sigma_y = \sqrt{\frac{1}{m} \sum_{k=1}^{m} (y[k] - y_{av})^2}, \quad y_{av} = \frac{1}{m} \sum_{k=1}^{m} y[k]. \quad (18)$$

And f_{av} can be determined by averaging the total number of the inverter legs' switching instants over a fixed period of time (10 ms in this work). These performance indices are also compared with those resulted using the simplified PMSM model to validate the analysis presented in Section III-B.

The sampling frequency is maintained at 20 kHz for consistency with the theoretical analysis. The hysteresis band limits of the torque and flux regulators needed for the pulse selectors (BST, MBST, AST, and ZST) are arbitrarily set to 2% of the rated torque and permanent magnet flux.

B. COMPARISON OF STEADY-STATE PERFORMANCE
Figs. 11 and 12 present the steady-state waveforms of torque, stator-flux amplitude, and average switching frequency obtained using the FEA-based and simplified models at different speeds and loading conditions.

As can be noticed in these figures, the performance prediction for all DTC strategies using the simplified model showed a considerably lower torque ripple at lower average switching frequencies (in most cases) than that employing the FEA-based model. In other words, the simplified model gives optimistic predictions of the steady-state performance compared to the FEA-based model due to neglecting the magnetic saturation, as discussed in Section III-B. These confirm the
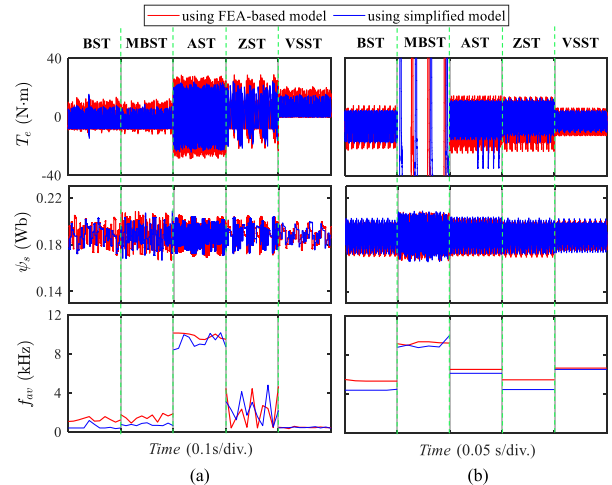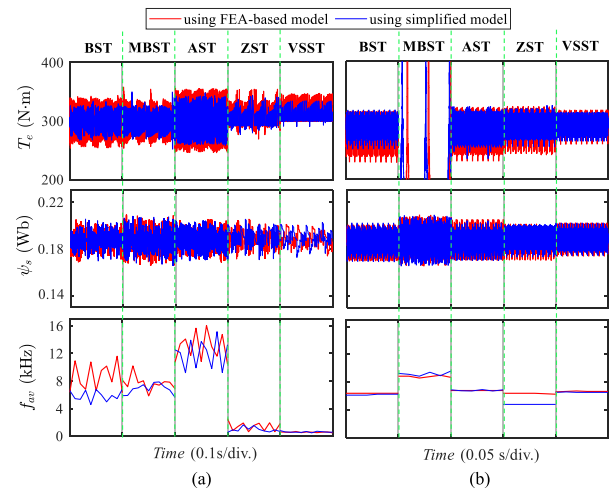

FIGURE 12. Simulation results of the steady-state performance at 75% of rated torque and different speeds. (a) At 100 r/min. (b) At 3000 r/min. [from top to bottom: torque T_e, stator-flux modulus ψ_s, and average switching frequency f_{av}].

necessity of employing the latter for performance prediction of DTC.

According to the FEA-based-model predictions of DTC performance shown in Figs. 11 and 12, the proposed VSST-based strategy outperforms the other methods regarding the torque and flux ripples, especially at high-speed (3000 r/min) or -loading conditions. Its average switching frequency is slightly higher than BST and ZST only at high-speed operation. The AST-based method produces the largest torque ripple with the highest average switching frequency because it uses the AVVs only, proving the importance of the ZVV inclusion in the look-up table. MBST can produce a lower torque ripple than BST and AST at the cost of a significant
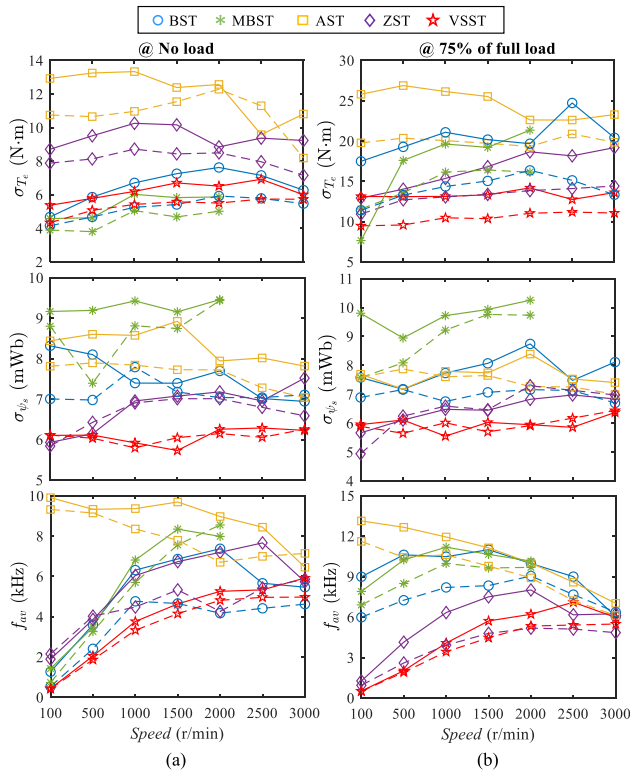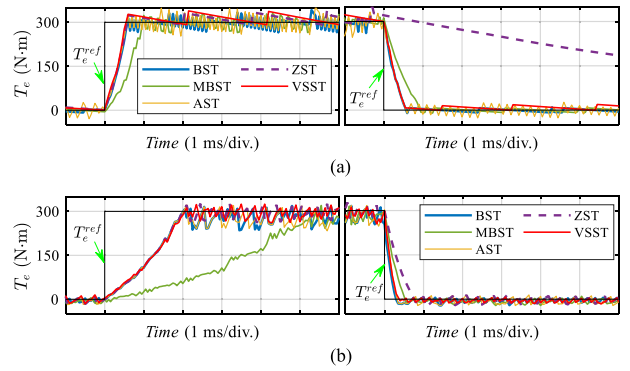
FIGURE 13. Quantitative evaluation of the steady-state performance at different operating speeds. (a) at no load. (b) at 75% of rated torque. [from top to bottom: torque ripple σ_{T_e}, stator-flux-amplitude ripple σ_{ψ_s}, and average switching frequency f_{av}; Solid line: using FEA-based model; Dashed line: using simplified model].

FIGURE 14. Simulation results of the torque dynamic response for DTC strategies with 300 N · m step at different operating speeds. (a) At 100 r/min. (b) At 3000 r/min (only MBST is tested at 2000 r/min).

rise in the flux ripple, as shown in Figs. 11(a) and 12(a). Also, as can be noticed in Figs. 11(b) and 12(b), MBST causes unstable operation at 3000 r/min speed because the voltage vector indexed $[n + 3]$ fails to increase the torque over a wide range of θ_s at high speeds [see Fig. 7(b)], as discussed in Section III-C

A detailed quantitative evaluations for σ_{T_e}, σ_{ψ_s}, and f_{av} under various operating speeds are given in Fig. 13 for no load and 75% of full load.

The simplified-model-based performance prediction showed that the proposed VSST produces a slightly higher torque ripple at no load than BST by average of 2% with almost the same average switching frequency. Also, at 0.75 of full load, it is detected that BST gives a lower torque ripple than MBST by around 0.5%. On the other hand, the FEA-model-based performance predictions indicated that the torque ripple produced by VSST is around 7% less than that of the BST with 25% lower average switching frequency at no load. At high load (0.75 of full load), MBST introduces lower torque ripple than BST by roughly 17% on average. For all DTC schemes under test, the simplified model predicts lower torque ripple and average switching frequency than the FEA-based model by averages of 22.5% and 17%, respectively. These results verify the analysis presented in

Section III-B and the need for employing the FEA model for DTC performance prediction.

From the FEA-model-based predictions presented in Fig. 13(a), the proposed VSST gives lower torque ripple at no load than AST and ZST by averages of 48%, and 34%, respectively. Although the proposed method produces higher torque ripple than MBST by around 12%, the flux ripple and the average switching frequency are dramatically reduced by averages of 35% and 30%, respectively. From Fig. 13(b), the torque ripple, flux ripple, and average switching frequency of the proposed strategy are the lowest at 75% of full load, which are respectively 30%, 18%, and 29%, on average, less than those of the other DTC schemes. These results verify the efficacy of the proposed VSST-based pulse selection strategy to enhance the steady-state performance of DTC.

C. COMPARISON OF THE DYNAMIC PERFORMANCE

Fig. 14 shows the FEA-model-based predictions of the torque dynamic performance when the demanded torque is stepped up from 0 to 300 N · m and down from 300 to 0 N · m under different rotor speeds, 100 and 3000 r/min.

Only MBST is tested at 2000 r/min instead of 3000 r/min to avoid the unstable operation mentioned in Section III-B.

It can be noticed in Fig. 14 that when the torque is increased, all the pulse selectors allow comparable torque responses for DTC, excluding MBST which causes slower torque dynamics. When the torque is stepped down, the dynamic response of ZST-DTC degrades significantly because of employing ZVV to decrease the torque, as discussed in Section III-C. This issue is avoided in the proposed strategy by applying AVVs during transient conditions.

By comparing Fig. 14(b) with Fig. 14(a), it can be noticed that the rising time increases at high speed (3000 r/min), while the falling time decays because the positive and negative torque deviations produced by AVVs weaken and strengthen, respectively, when the speed rises. Furthermore, it can be noticed in Fig. 14(b) that the falling time is shorter than the rising time as the negative deviations in torque is larger than the positive deviations when ω_r is positive [see Fig. 7(b)].

(a)

(b)
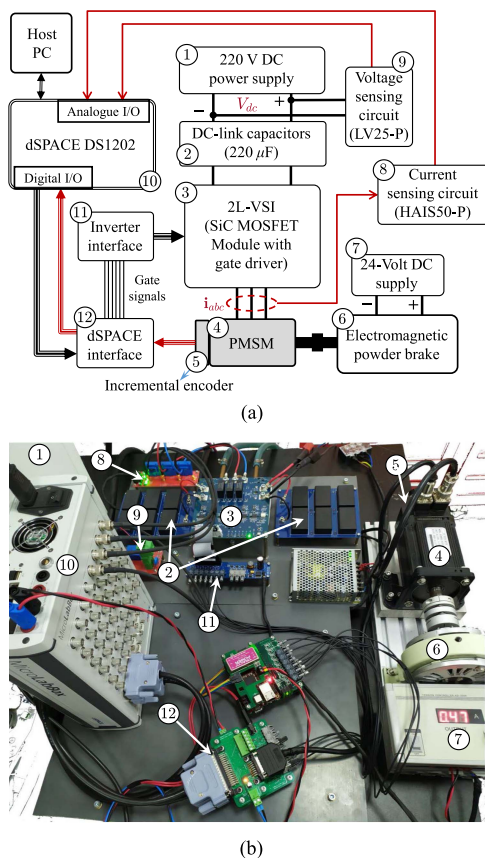
FIGURE 15. Experimental setup. (a) Block diagram. (b) Photo of the test bench.

These simulation results are consistent with the theoretical analysis presented in Section III-C and confirm that the proposed VSST-based pulse selection strategy can retain the fast dynamic response of DTC.

VI. EXPERIMENTAL VERIFICATION

In this section, the experimental results are presented to verify the outcomes of the comparative analysis presented in Section III-C and the effectiveness of the proposed method [Section IV] under different operating conditions. As the pulse selectors are the main focus of this article, a 0.75-kW SPMSM (with the parameters are listed in the Appendix) can be a feasible option for the experimental verification to avoid the implementation complexity and the stability issues associated with flux estimation of IPMSM [42], [43].

As shown in Fig. 15, the motor is fed from 220-Volt DC supply and 200-μF DC-link capacitors through a 2L-VSI. Two LEM sensors detects the stator-winding currents and the DC-link voltage, while an incremental encoder with a precision of 2500 pulse per revolution determines the rotor angular position. The motor shaft is mechanically coupled to a powder brake supplied by a 24-Volt variable DC source to manipulate the load torque.

Two software are used to realize the experimental implementation of the DTC strategies. Before the experiment,

Matlab/Simulink is utilized to establish a model for the control algorithm under test and generate the corresponding control code. Then, dSPACE ControlDesk is utilized to download the code to the controller processing unit and directly change the reference signals and control parameters through the host PC. It is also employed to capture the experimental results for post processing, analysis, and drawing using Matlab. The sampling period is maintained at 50 μs. For the sake of accuracy, the one-step delay due to the digital implementation is remedied for all the DTC strategies such that the switching pulse is selected based on the predicted torque and flux at the $(k+1)$th sampling instant [44].
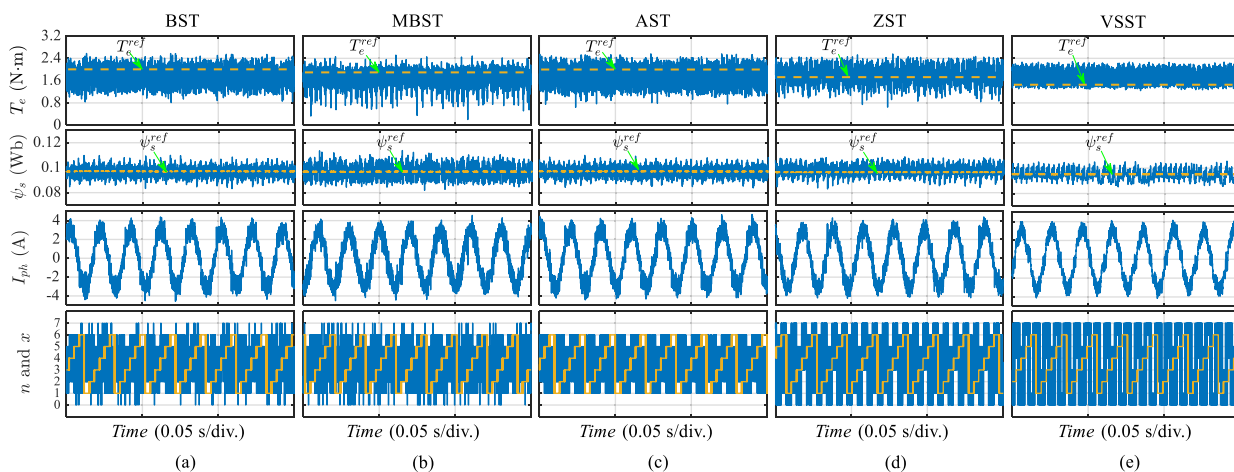
A. STEADY-STATE PERFORMANCE TESTS

Figs. 16 and 17 represent the experimental waveforms of electromagnetic torque, stator-flux amplitude, phase current, and the selected-vector index for the DTC schemes at 750 r/min and 2250 r/min, respectively. As the MBST exhibits unstable operation at 2250 r/min, it is tested at 1500 r/min instead. The load torque is maintained at around 1.8 N $\cdot$ m. To maintain the speed at a constant value while capturing the experimental results using the ControlDesk, the demanded torque is generated by an outer PI-speed loop with gains of $K_P = 0.006843$ and $K_I = 0.78046$. For better efficiency, the maximum torque per ampere principle is used to calculate the reference stator-flux amplitude from the demanded torque [14].

From Figs. 16 and 17, it can be observed that the proposed VSST-based method provides a significant reduction in torque ripple and current distortions compared to the other pulse selectors as it avoids selecting the AVVs that give high deviations in torque during steady-state operation, as discussed in Section IV. Although the application of MBST for DTC causes less torque ripple than BST and AST, it produces higher flux ripple. The ZST improves both the torque and flux ripples compared with BST and AST because of the more frequently employed ZVV, as can be noticed from the vector-index waveform.

Fig. 18 presents a quantitative evaluation for the steady-state performance of DTC under different pulse selectors in terms of torque ripple, flux ripple, average switching frequency, and total harmonic distortion of the stator current (THD$_I$). The torque ripple of the proposed VSST is significantly less than that of BST, MBST, AST, and ZST by averages of 46%, 44%, 48%, and 41%, respectively. Furthermore, the proposed method achieves the lowest flux ripple, current distortions, and average switching frequency that are respectively reduced by 16%, 19%, and 37%, on average, compared with the other methods. On the other hand, MBST can mitigate the torque ripple at low speed (750 r/min) by about 6% with 16% lower average switching frequency compared to BST, but the stator flux ripple and the current distortion increase by 24% and 4%, respectively. These results match well with the performance analysis and the simulation results presented in Sections III-C and V-B, respectively.

To further verify the superiority of the proposed method, it is compared with the BST-based pulse selector with different

FIGURE 16. Experimental results of the steady-state performance for DTC strategies under 1.8-N · m load and 750-r/min speed. (a) BST. (b) MBST. (c) AST. (d) ZST. (e) VSST. [from top to bottom: torque, stator-flux amplitude, phase current, sector n and selected voltage vector x].
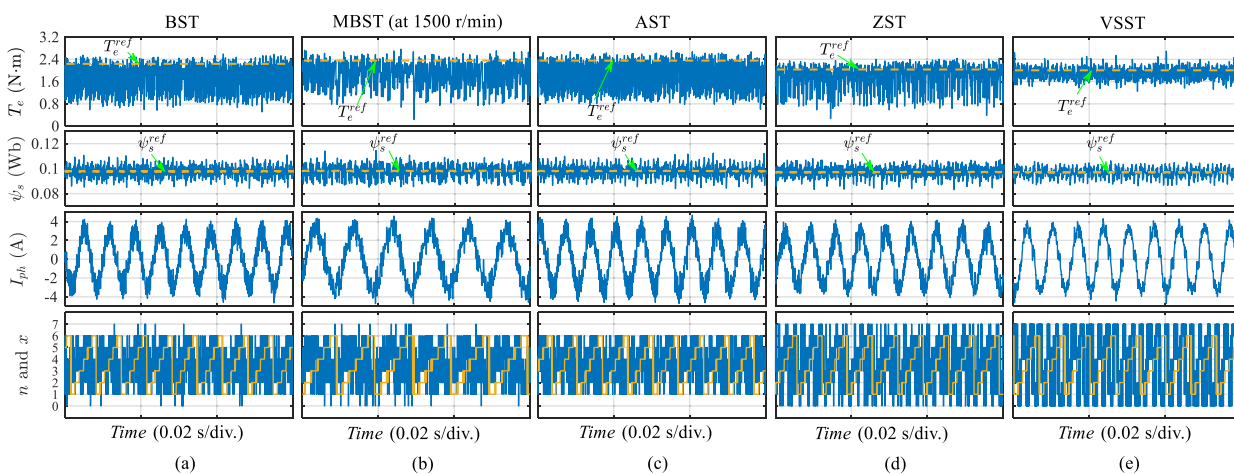
FIGURE 17. Experimental results of the steady-state performance for DTC strategies under 1.8-N · m load and 2250-r/min speed. (a) BST. (b) MBST (at 1500 r/min). (c) AST. (d) ZST. (e) VSST. [from top to bottom: torque, stator-flux amplitude, phase current, sector n and selected voltage vector x].

values of hysteresis band limits of the torque regulator ($\pm h_{T_e}$), as shown in Fig. 19. In this test, the load torque is set to 1.8 N · m, and the speed is maintained around 750 r/min. From the vector index x in Fig. 19, the frequency of employing the ZVV (0 or 7) increases when the h_{T_e} is increased from 2% to 10% of the rated torque, resulting in reduced torque ripple and current distortion with lower average switching frequency. As the proposed strategy applies ZVV at the look-up table state ($\varepsilon_{T_e} = \downarrow$) instead of AVV, it can hit the maximum possible frequency of employing the ZVVs. Consequently, the proposed VSST scheme can always provide a lower torque ripple with reduced average switching frequency than BST regardless of the value of the torque-hysteresis band limits ($\pm h_{T_e}$).

B. DYNAMIC PERFORMANCE TESTS

The torque dynamic responses of DTC under different pulse selectors are also investigated and compared, as shown in Fig. 20. For these experiments, the motor is operated in torque

control mode with a fixed load toque at around 1.6 N · m. The demanded torque is stepped up from 0 to 2 N · m to test the torque dynamic performance during start up. Then, once the velocity hits the value of 1500 r/min, the demanded torque is stepped down from 2 to −2 N · m to investigate the torque behavior during speed reversal. The corresponding speed response and phase current of the PMSM for that test scenario are illustrated to the bottom of the torque response. The zoomed zones ① and ② in Fig. 20 show the rise and fall time of the torque responses.

In Fig. 20, it can be noticed that BST, AST, ZST, and the proposed VSST achieve fast torque response with a rise time of 0.2 ms, approximately. On the other hand, the torque dynamic response is slightly slower for MBST (almost 0.27 ms) as it uses the sector definition n_2 (7) where the AVVs give lower deviations in torque than that with n_1 (6) [see Fig. 7]. When the demanded torque was changed from 2 to −2 N · m, the falling time of the torque
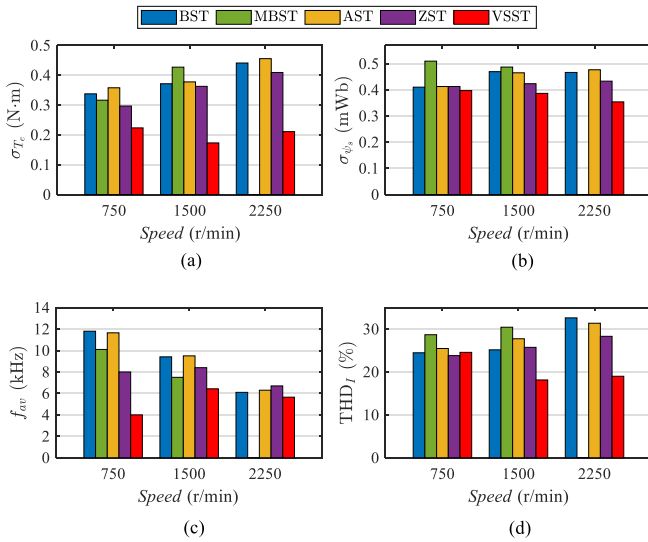
FIGURE 18. Quantitative evaluation of the steady-state performance for DTC strategies under 1.8 N · m-load torque at different operating speeds. (a) Torque ripple. (b) Flux ripple. (c) Average switching frequency. (d) Total harmonic distortion of stator current. [Experimental results].
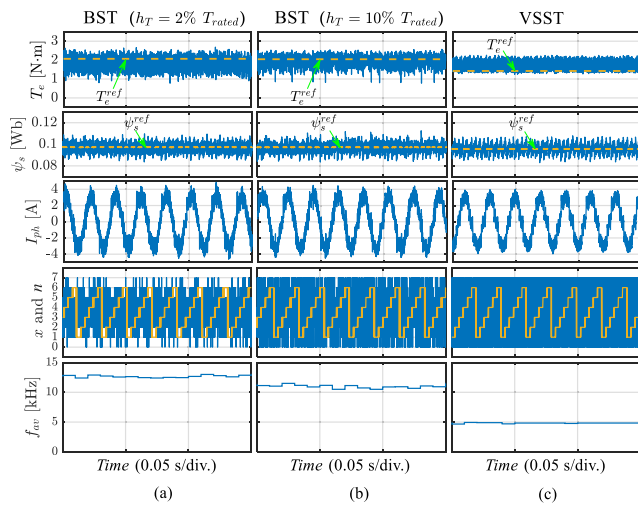

FIGURE 19. Experimental waveforms of the torque, flux amplitude, phase current, and index of the selected voltage vector at 750 r/min. (a) BST at $h_T = 2\% \, T_{rated}$. (b) BST at $h_T = 10\% \, T_{rated}$. (c) Proposed VSST.

for all the employed pulse selectors was around 0.27 ms except ZST, the torque response of which needed about 0.55 ms to match the demanded value. Moreover, during speed reversal, the ZST causes system instability when the operating speed reaches zero, as shown in Fig. 20(d), because the torque variation direction of the ZVVs reverses [see Fig. 16(c)]. Instead, the proposed VSST provides faster response during torque-demand decay (because it employs only the AVVs during the dynamic state), and it can achieve smooth speed reversal, as can be noticed in Fig. 20(e). After speed reversal, it can satisfy a steady-state performance identical to that during

TABLE 3. Summary of the Comparative Investigation of DTC Performance Under Different Pulse Selectors

| Performance indices	BST	MBST	AST	ZST	VSST
Torque ripple	★★☆	★★☆	★☆☆	★★☆	★★★
Flux ripple	★★☆	★☆☆	★★☆	★★☆	★★★
Average switching frequency	★☆☆	★★☆	★☆☆	★★☆	★★★
Rising-torque response	★★★	★★☆	★★★	★★★	★★★
Falling-torque response	★★★	★★☆	★★★	★☆☆	★★★
Speed reversal	★★★	★★★	★★★	☆☆☆	★★★
Implementation complexity	★★☆	★★☆	★★☆	★★☆	★★★

the forward operation by changing the switching-table structure. These results confirm well with the performance analysis and the simulation results presented in Sections III-C and V-C, respectively, and show that the proposed VSST-based pulse selection strategy can keep the fast dynamic performance of DTC with smooth speed reversal and reduced torque and flux ripples.

C. DISCUSSION

The criteria of pulse selection without considering the application of ZVVs in DTC, such as the AST-based method, results in excessive torque and flux ripples with high average switching frequency. Therefore, by employing three-level torque hysteresis regulators in both BST and MBST, the torque ripple and average switching frequency can be reduced by increasing how frequently the ZVVs are selected. However, the latter results in increased flux ripple, instability at high-speed operation, and degraded dynamic torque response because it uses a sector definition n_2 (7) where the switching pulses give high deviations in flux amplitude, low torque deviations, and they fail to increase the torque at high-speed conditions. Although applying a ZVV at a single table state in ZST can also reduce the torque ripple, the speed reversal is not allowed because the torque deviations produced by ZVV reverse with the rotational direction. The proposed VSST strategy overcomes all these performance issues due to its flexibility of pulse selection with the operating state and direction of rotation. It achieves the lowest torque and flux ripples with reduced average switching frequency while retaining the fast dynamic response of DTC. Table 3 summarizes the comparative evaluation of the DTC performance under the different pulse selectors discussed in this work. The superiority of a particular pulse selector for a particular performance index is ranked such that ★★★ illustrates the highest superiority.

VII. CONCLUSION

In this article, a generalized performance analysis using a high-fidelity FEA-based model is presented to investigate the impact of the pulse selection criteria on the DTC performance of three-phase PMSM drives, including nonlinear machine behavior such as magnetic saturation. Different pulse selectors are theoretically analyzed to identify the performance issues for both steady-state and dynamic operating conditions. By considering the operating state in the pulse selection
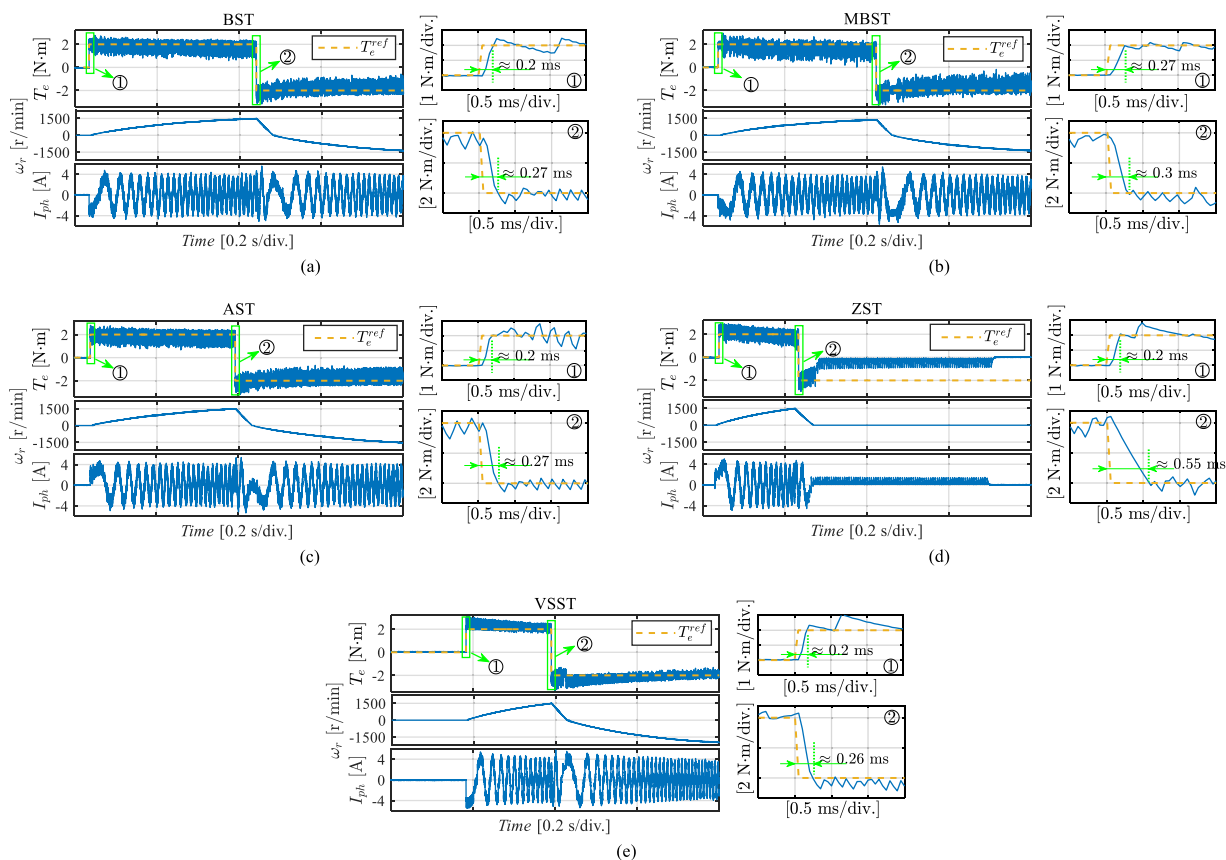
FIGURE 20. Experimental results of the torque dynamic performance for DTC under different pulse selectors when the torque is stepped up from 0 to 2 N · m and down from 2 to −2 N · m. (a) BST. (b) MBST. (c) AST. (d) ZST. (e) VSST. [from top to bottom: electromagnetic torque, rotor speed, and phase current].

criteria, the torque and flux ripples can be minimized while maintaining robustness and fast torque dynamics. Therefore, a VSST-based pulse selector is proposed, where the voltage vectors that produce relatively low deviations in torque and flux are employed during steady-state operation, while those of them that give high variation rates are applied during system dynamics. A detailed comparative evaluation for the DTC performance under different pulse selectors is presented using both simulations and experiments, which conform well with the theoretical analysis and verify the effectiveness of the proposed strategy.

The FEA-based model can be utilized for performance investigation of DTC considering other nonlinear characteristics, such as thermal or cogging effects or other control scenarios like different fault conditions. These can help identify new methodologies for pulse selection in DTC, as will be further demonstrated in future studies.

APPENDIX
The electrical parameters of the machines used for simulation and experimental verification in this work are presented in Table 4.

TABLE 4. List of PMSM Parameters

Parameters	IPMSM	SPMSM	Units
Rated power	80	0.75	kW
Stator-phase resistance (R_s)	7.5e-3	0.901	Ω
d-axis inductance (L_d)	0.6	6.552	mH
q-axis inductance (L_d)	1.33	6.552	mH
Number of pole pairs (p)	4	4	-
Rated torque	400	2.4	N·m
Base speed	3000	3000	r/min
Rated current	-	4.2	A
Peak current	400	-	A
DC-link voltage (V_{dc})	540	220	Volt
Inertia coefficient (J)	0.16526	1.2e-4	kg·m^2
Permanent magnet flux (ψ_{pm})	0.1875	0.09427	Wb

REFERENCES
[1] M. Kashif and B. Singh, "Modified active-power MRAS based adaptive control with reduced sensors for PMSM operated solar water pump," *IEEE Trans. Energy Convers.*, vol. 38, no. 1, pp. 38–52, Mar. 2023.
[2] S. Walz and M. Liserre, "Hysteresis model predictive current control for PMSM with LC filter considering different error shapes," *IEEE Open J. Power Electron.*, vol. 1, pp. 190–197, 2020.

[3] L. Zhong, M. Rahman, W. Hu, and K. Lim, "Analysis of direct torque control in permanent magnet synchronous motor drives," *IEEE Trans. Power Electron.*, vol. 12, no. 3, pp. 528–536, May 1997.

[4] S. A. A. Tarusan, A. Jidin, and M. L. M. Jamil, "The optimization of torque ripple reduction by using DTC-multilevel inverter," *ISA Trans.*, vol. 121, pp. 365–379, 2022.

[5] M. F. Rahman, L. Zhong, M. Haque, and M. A. Rahman, "A direct torque- controlled interior permanent-magnet synchronous motor drive with- out a speed sensor," *IEEE Trans. Energy Convers.*, vol. 18, no. 1, pp. 17–22, Mar. 2003.

[6] M. Gu, Z. Wang, C. Wen, and Z. Zou, "Collaborative mid-point voltage regulation in low-switching-frequency MPC for three-level NPC inverters fed dual three-phase PMSM drives," *IEEE Open J. Power Electron.*, vol. 2, pp. 673–682, 2021.

[7] A. Poorfakhraei, M. Narimani, and A. Emadi, "A review of multilevel inverter topologies in electric vehicles: Current status and future trends," *IEEE Open J. Power Electron.*, vol. 2, pp. 155–170, 2021.

[8] W. Deng and S. Zuo, "Electromagnetic vibration and noise of the permanent-magnet synchronous motors for electric vehicles: An overview," *IEEE Trans. Transport. Electrific.*, vol. 5, no. 1, pp. 59–70, Mar. 2019.

[9] H. Yuwen, T. Cun, G. Yikang, Y. Zhiqing, L. X. Tang, and M. F. Rahman, "In-depth research on direct torque control of permanent magnet synchronous motor," in *Proc. IEEE 28th Annu. Conf. Ind. Electron. Soc.*, 2002, vol. 2, pp. 1060–1065.

[10] S. B. H. Toufouti and R. Meziane, "Direct torque control strategy of induction motors," *Acta Electrotechnica et Informatica*, vol. 7, no. 1, pp. 22–28, 2007.

[11] Y. Li, D. Gerling, and W. Liu, "A novel switching table using zero voltage vectors for direct torque control in permanent magnet synchronous motor," in *Proc. 18th Int. Conf. Elect. Mach.*, 2008, pp. 1–6.

[12] C. Xia, S. Wang, Z. Wang, and T. Shi, "Direct torque control for VSI-PMSMs using four-dimensional switching-table," *IEEE Trans. on Power Electron.*, vol. 31, no. 8, pp. 5774–5785, Aug. 2016.

[13] A. Taheri, "Harmonic reduction of Direct Torque Control of six-phase induction motor," *ISA Trans.*, vol. 63, pp. 299–314, 2016.

[14] Y. Zhang and J. Zhu, "Direct torque control of permanent magnet synchronous motor with reduced torque ripple and commutation frequency," *IEEE Trans. Power Electron.*, vol. 26, no. 1, pp. 235–248, Jan. 2011.

[15] Y. Ren, Z. Q. Zhu, and J. Liu, "Direct torque control of permanent-magnet synchronous machine drives with a simple duty ratio regulator," *IEEE Trans. Ind. Electron.*, vol. 61, no. 10, pp. 5249–5258, Oct. 2014.

[16] F. Niu, K. Li, and Y. Wang, "Direct torque control for permanent-magnet synchronous machines based on duty ratio modulation," *IEEE Trans. Ind. Electron.*, vol. 62, no. 10, pp. 6160–6170, Oct. 2015.

[17] F. Niu et al., "A simple and practical duty cycle modulated direct torque control for permanent magnet synchronous motors," *IEEE Trans. Power Electron.*, vol. 34, no. 2, pp. 1572–1579, Feb. 2019.

[18] A. Nasr, C. Gu, X. Wang, G. Buticchi, S. Bozhko, and C. Gerada, "Torque-performance improvement for direct torque-controlled PMSM drives based on duty-ratio regulation," *IEEE Trans. Power Electron.*, vol. 37, no. 1, pp. 749–760, Jan. 2022.

[19] W. Chen, S. Zeng, G. Zhang, T. Shi, and C. Xia, "A modified double vectors model predictive torque control of permanent magnet synchronous motor," *IEEE Trans. Power Electron.*, vol. 34, no. 11, pp. 11419–11428, Nov. 2019.

[20] Z. Song, X. Ma, and R. Zhang, "Enhanced finite-control-set model predictive flux control of permanent magnet synchronous machines with minimum torque ripples," *IEEE Trans. Ind. Electron.*, vol. 68, no. 9, pp. 7804–7813, Sep. 2021.

[21] F. Niu, B. Wang, A. S. Babel, K. Li, and E. G. Strangas, "Comparative evaluation of direct torque control strategies for permanent magnet synchronous machines," *IEEE Trans. Power Electron.*, vol. 31, no. 2, pp. 1408–1424, Feb. 2016.

[22] E. Kusuma, K. M. R. Eswar, and T. V. Kumar, "An effective predictive torque control scheme for PMSM drive without involvement of weighting factors," *IEEE Trans. Emerg. Sel. Topics Power Electron.*, vol. 9, no. 3, pp. 2685–2697, Jun. 2021.

[23] F. Wang, H. Xie, Q. Chen, S. A. Davari, J. Rodríguez, and R. Kennel, "Parallel predictive torque control for induction machines without weighting factors," *IEEE Trans. Power Electron.*, vol. 35, no. 2, pp. 1779–1788, Feb. 2020.

[24] A. Nasr, C. Gu, S. Ijaz, G. Buticchi, S. Bozhko, and C. Gerada, "Sequential finite-element-based model predictive torque and flux control method for IPMSM," in *Proc. 5th Int. Conf. Energy, Elect. Power Eng.*, 2022, pp. 1081–1086.

[25] X. Li, Z. Xue, X. Yan, L. Zhang, W. Ma, and W. Hua, "Low-complexity multivector-based model predictive torque control for PMSM with voltage preselection," *IEEE Trans. Power Electron.*, vol. 36, no. 10, pp. 11726–11738, Oct. 2021.

[26] C. Ma et al., "A novel torque boundary-based model predictive torque control for PMSM without weighting factor," *IEEE Trans. Emerg. Sel. Topics Power Electron.*, vol. 9, no. 4, pp. 4395–4406, Aug. 2021.

[27] A. Nasr, C. Gu, G. Buticchi, S. Bozhko, and C. Gerada, "A low-complexity modulated model predictive torque and flux control strategy for PMSM drives without weighting factor," *IEEE Trans. Emerg. Sel. Topics Power Electron.*, vol. 11, no. 2, pp. 1305–1316, Apr. 2023.

[28] J. Li, W. Song, B. Liu, J. Guo, Y. Wu, and Y. Li, "A comparative study of current harmonics and switching frequency with different pulse patterns in duty-cycle-based model predictive current control," *IEEE Trans. Ind. Electron.*, vol. 70, no. 11, pp. 10891–10901, Nov. 2023.

[29] D. Swierczynski and M. Kazmierkowski, "Direct torque control of permanent magnet synchronous motor (PMSM) using space vector modulation (DTC-SVM)-simulation and experimental results," in *Proc. IEEE 28th Annu. Conf. Ind. Electron. Soc.*, 2002, vol. 1, pp. 751–755.

[30] J. S. Lee, C. -H. Choi, J. -K. Seok, and R. D. Lorenz, "Deadbeat-direct torque and flux control of interior permanent magnet synchronous machines with discrete time stator current and stator flux linkage observer," *IEEE Trans. Ind. Appl.*, vol. 47, no. 4, pp. 1749–1758, Jul./Aug. 2011.

[31] W. Wang, C. Liu, H. Zhao, and Z. Song, "Improved deadbeat-direct torque and flux control for PMSM with less computation and enhanced robustness," *IEEE Trans. Ind. Electron.*, vol. 70, no. 3, pp. 2254–2263, Mar. 2023.

[32] C. Lascu, A. Argeseanu, and F. Blaabjerg, "Supertwisting sliding-mode direct torque and flux control of induction machine drives," *IEEE Trans. Power Electron.*, vol. 35, no. 5, pp. 5057–5065, May 2020.

[33] P. Karamanakos and T. Geyer, "Guidelines for the design of finite control set model predictive controllers," *IEEE Trans. Power Electron.*, vol. 35, no. 7, pp. 7434–7450, Jul. 2020.

[34] X. Chen, J. Wang, B. Sen, P. Lazari, and T. Sun, "A high-fidelity and computationally efficient model for interior permanent-magnet machines considering the magnetic saturation, spatial harmonics, and iron loss effect," *IEEE Trans. Ind. Electron.*, vol. 62, no. 7, pp. 4044–4055, Jul. 2015.

[35] N. Bracikowski, M. Hecquet, P. Brochet, and S. V. Shirinskii, "Multiphysics modeling of a permanent magnet synchronous machine by using lumped models," *IEEE Trans. Ind. Electron.*, vol. 59, no. 6, pp. 2426–2437, Jun. 2012.

[36] N. Nakao and K. Akatsu, "Suppressing pulsating torques: Torque ripple control for synchronous motors," *IEEE Ind. Appl. Mag.*, vol. 20, no. 6, pp. 33–44, Nov./Dec. 2014.

[37] H. Kaimori, N. Nakao, T. Sakaue, and K. Akatsu, "Behavior modeling of permanent magnet synchronous motors using flux linkages for coupling with circuit simulation," in *Proc. Int. Conf. Elect. Machines*, 2014, pp. 2695–2701.

[38] C. Lai, G. Feng, K. Mukherjee, V. Loukanov, and N. C. Kar, "Torque ripple modeling and minimization for interior PMSM considering magnetic saturation," *IEEE Trans. Power Electron.*, vol. 33, no. 3, pp. 2417–2429, Mar. 2018.

[39] X. Chen, J. Wang, and A. Griffo, "A high-fidelity and computationally efficient electrothermally coupled model for interior permanent-magnet machines in electric vehicle traction applications," *IEEE Trans. Transport. Electrific.*, vol. 1, no. 4, pp. 336–347, Dec. 2015.

[40] J. D'Errico, "Surface fitting using gridfit," Matlab Central Files Exchange. [Online]. Available: https://www.mathworks.com/matlab central/fileexchange/8998-surface-fitting-using-gridfit

[41] A. Nasr, C. Gu, W. Zhao, S. Bozhko, and C. Gerada, "Torque ripple suppression for IPMSM using FEA- based model predictive direct torque control," in *Proc. IEEE Workshop Elect. Mach. Des., Control Diagnosis*, 2021, pp. 204–209.

[42] M. Rahman, M. Haque, L. Tang, and L. Zhong, "Problems associated with the direct torque control of an interior permanent-magnet synchronous motor drive and their remedies," *IEEE Trans. Ind. Electron.*, vol. 51, no. 4, pp. 799–809, Aug. 2004.

[43] Z. Q. Zhu, D. Liang, and K. Liu, "Online parameter estimation for permanent magnet synchronous machines: An overview," *IEEE Access*, vol. 9, pp. 59059–59084, 2021.

[44] Y. Zhang, J. Zhu, and W. Xu, "Analysis of one step delay in direct torque control of permanent magnet synchronous motor and its remedies," in *Proc. Int. Conf. Elect. Mach. Syst.*, 2010, pp. 792–797.

AHMED NASR was born in Cairo, Egypt, in 1988. He received the B.Sc. (Hons.) and M.Sc. degrees in electrical engineering from Zagazig University, Zagazig, Egypt, in 2010 and 2015, respectively, and the Ph.D. degree in electrical and electronic engineering from the University of Nottingham, Nottingham, U.K., in 2023. He is currently a Postdoc Researcher with the Key Laboratory of More Electric Aircraft Technology of Zhejiang Province, University of Nottingham Ningbo, Ningbo, China. From 2011 to 2018, he was a Research and Teaching Assistant with the Department of Electrical Power and Machines, Zagazig University. His research interests include modeling and control of electric drives and renewable energy systems.

CHUNYANG GU (Senior Member, IEEE) received the B.Sc. degree in electrical engineering from the Harbin Institute of Technology, Harbin, China, in 2010, and the Ph.D. degree in electrical engineering from the Tsinghua University, Beijing, China, in 2015. She was a Postdoc Research Fellow with the Power Electronics, Machines and Control Research Group, University of Nottingham, Nottingham, U.K., from 2015 to 2017. In 2017, she joined the Department of Electrical and Electronic Engineering, University of Nottingham Ningbo China, Ningbo, China, as an Assistant Professor. She is currently an Associate Professor with the same department. She was appointed as a Research Professor with the Advanced Electrical Machine Drive Research Center, Yongjiang Laboratory, Ningbo, in 2023. Her research interests include power electronics for transportation electrification, renewable energy, and grid applications.

JING LI (Senior Member, IEEE) received the B.Eng. and M.Sc. degrees (Hons.) in electrical and electronic engineering from the Beijing Institute of Technology, Beijing, China, in 1999 and 2002, respectively, and the Ph.D. degree in electrical and electronic engineering from the University of Nottingham, Nottingham, U.K., in 2010. She was a Research Fellow after graduation with the Power Electronics, Machine and Control Group, University of Nottingham. In 2016, she was an Assistant Professor with the University of Nottingham Ningbo China, Ningbo, China, where she is currently an Associate Professor with the Department of Electrical and Electronic Engineering. Her research interests include condition monitoring for motor drive systems and power distribution systems, advanced control, and design of motor drive systems.

GIAMPAOLO BUTICCHI (Senior Member, IEEE) received the master's degree in electronic engineering and the Ph.D. degree in information technologies from the University of Parma, Parma, Italy, in 2009 and 2013, respectively. Between 2014 and 2017, he was a Postdoctoral Researcher and Guest Professor with the University of Kiel, Kiel, Germany. He is currently a Professor in electrical engineering with the Nottingham University Ningbo China, Ningbo, China, and the Associate Dean for Research and Knowledge Exchange of the Faculty of Science and Engineering. His research interests include power electronics for renewable energy systems, smart transformer fed microgrids, and dc grids for the more electric aircraft.

SALMAN IJAZ received the Ph.D. degree in control sciences and engineering from Beihang University, Beijing, in 2018. Between 2018 and 2020, he was a Postdoctoral Researcher with the Nanjing University of Aeronautics and Astronautics, Nanjing, China. Since December 2020, he was appointed as an Assistant Professor with the School of Aerospace, University of Nottingham, Ningbo, China. He is also a member of the Key Laboratory of More Electric Aircraft Zhejiang Province and the Control Systems Laboratory. His current research interests include the fault-tolerant control of aircraft systems, sliding mode control, control allocations, and UAV systems.

CHRIS GERADA (Senior Member, IEEE) received the Ph.D. degree in the numerical modeling of electrical machines from the University of Nottingham, Nottingham, U.K., in 2005. He was a Researcher with the University of Nottingham on high-performance electrical drives and on the design and modeling of electromagnetic actuators for aerospace application. Since 2006, he has been a Project Manager with the GE Aviation Strategic Partnership, Cincinnati, OH, USA. In 2008, he was a Lecturer in electrical machines, in 2011, an Associate Professor, and in 2013, a Professor with the University of Nottingham. His research interest includes the design and modeling of high-performance electric drives and machines.

HE ZHANG (Senior Member, IEEE) received the B.Eng. degree in control science and engineering from Zhejiang University, Hangzhou, China, in 2002, and the M.Sc. and Ph.D. degrees in electrical machines from The University of Nottingham, Nottingham, U.K., in 2004 and 2009, respectively. He was a Research Fellow with the University of Nottingham, U.K. and the Director of BestMotion Technology Centre. He moved to the University of Nottingham Ningbo China, Ningbo, China, as Senior Research Fellow in 2014, promoted to Principal Research Fellow in 2016 and to Professor in 2020. He is currently the Director of Nottingham Electrification Centre within the Power electronics, Machines and Control Research Group, University of Nottingham. His research interests include high-performance electric machines and drives for transport electrification.